Fall 2013

An evaluation of de-embedding techniques for TSVs

Nicholas Garrett Erickson

Department: Electrical and Computer Engineering

AN EVALUATION OF DE-EMBEDDING TECHNIQUES FOR TSVS

by

NICHOLAS GARRETT ERICKSON

A THESIS

Presented to the Graduate Faculty of the

MISSOURI UNIVERSITY OF SCIENCE AND TECHNOLOGY

In Partial Fulfillment of the Requirements for the Degree

MASTER OF SCIENCE IN COMPUTER ENGINEERING

2013

Approved by

Jun Fan, Advisor
Daryl Beetner
Yiyu Shi

ABSTRACT

One of the most important aspects of modern electronic designs is device measurement and characterization. Without device measurement and characterization, the functionality of end designs cannot be guaranteed. At the silicon level (on-wafer), extracting the electrical performance of devices and structures has grown increasingly more complex with the continual shrink of feature sizes. Compared to the overall measurement setup (VNA, cables, probes, interposers, etc.), the ultra small size of on-wafer structures leads to their electrical performance being easily overshadowed by other, larger fixtures. Thus, many scientists and engineers have worked to devise ever more accurate calibration and de-embedding techniques for measurement setups.

This thesis explores current state-of-the-art de-embedding techniques for both silicon transmission lines and general devices under test (DUTs). A complete evaluation is performed on several techniques, leading to a best choice selection for use in de-embedding through-silicon-vias (TSVs). During the evaluation a more intuitive approach (utilizing scattering parameters) is taken to verify the accuracy of the various de-embedding techniques. Attempts at formulating new de-embedding techniques are also explored.

ACKNOWLEDGMENTS

I would like to express my sincere gratitude to my advisor, Dr. Jun Fan, for his constant support and invaluable advice throughout my master's program. I would especially like to thank him for keeping me on track during the times when I became frustrated. I would also like to thank Dr. Daryl Beetner for one, advising me through the later portion of my undergraduate program; two, getting me started with research; and three, serving on my committee for this thesis. To Dr. Yiyu Shi, I thank you for your willingness to serve on my committee.

To everyone at the EMC Lab, I thank you for your friendship, your support, and your mentoring. I would especially like to thank Ketan for teaching me all the fundamentals during my beginning days at the EMC Lab.

To my parents, sisters, and brother: I could not succeed without your unconditional and unending support, love, and encouragement. To my friends: thank you for sharing in this journey with me. Additionally, I thank God for making all that we have possible, and for leaving so much for us to explore. Finally, thank you to Cisco for funding the research in this thesis.

TABLE OF CONTENTS

LIST OF ILLUSTRATIONS

1. INTRODUCTION

1.1 BACKGROUND

1.1.1 Network Analyzer Beginnings. The invention of semiconductor devices revolutionized the world of electronics. Without semiconductor devices, the technology of today would not be possible. Not surprisingly, with the onslaught of electronic designs using semiconductor devices, came a need to measure and characterize said devices. Thus, the first network analyzer, capable of swept amplitude and phase measurements, entered the market. During the same time, the theory and use of scattering parameters was conceptualized and popularized.

Since the network analyzer allowed for high frequency measurements, and thus enabled high frequency designs, many scientists and engineers worked to keep improving its capabilities. The same is true today as the vector network analyzer (VNA), the modern form of the network analyzer, is unsurpassed in accuracy when it comes to making radio-frequency (RF) measurements. The power of VNA measurements, however, can only be realized through proper use of calibration and de-embedding techniques; perhaps the most popular topics that continue to be studied with network analyzers. It must be noted that, although similar, calibration and de-embedding are not the same.

1.1.2 Calibration Overview. Calibration typically shifts the reference plane of the measurement up to the test vehicle for the device under test (DUT) by mathematically removing the effects of cables and adapters. By characterizing cables and adapters as error networks, using any of the network parameter sets (S, ABCD, or T) to represent the aforementioned error networks, a system of equations can be constructed. Depending on the overall error model employed, a certain number of

unknowns, outnumbering the available number of equations, will be contained within the system of equations. To solve for these unknowns, and thereby fully characterize the error networks, more equations must be generated.

The additional equations are usually generated by connecting various load conditions to the end of the error networks. Precision shorts, opens, loads, and lines are most often utilized to create the needed load conditions. Drawing from the nature of the load conditions are the so named short-open-load-thru (SOLT) calibration, thru-reflect-line (TRL) calibration, and thru-reflect-match (TRM) calibration, to name a few.

The important point to notice is that calibration rarely shifts the reference planes entirely to the edges of the DUT. Errors arising from test fixtures and other measurement structures that are required only for measurement (and not for the end implementation of the DUT), cannot typically be accounted for in the calibration process. Figure 1.1 gives a simple illustration of where the measurement reference plane is shifted to after a successful calibration, for measurements involving micro-probes.

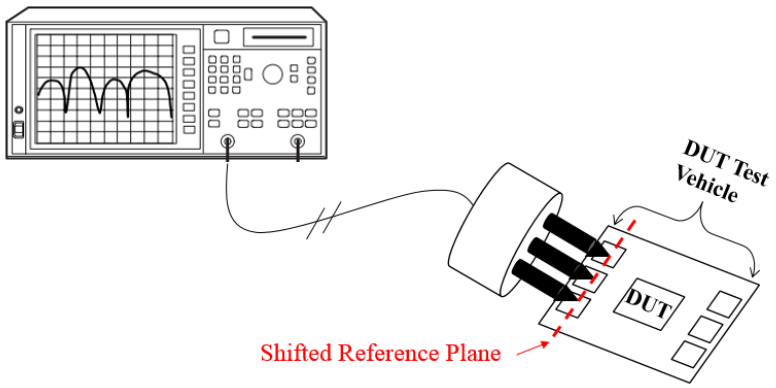

Figure 1.1: Example Location of Reference Plane After Calibration

1.1.3 De-embedding Overview. De-embedding attempts to remove measurement parasitics that cannot be accounted for through calibration, ideally shifting the measurement reference plane all the way up to the edge of the DUT, as shown in Figure 1.2. Conversely to calibration, de-embedding does not occur during the measurement process; instead, it is purely a post-processing action. De-embedding is similar to calibration in the essence that unknown error terms must be fully characterized from some total system, or manipulations of that total system. One way to view calibration and de-embedding is as a two-tiered approach to error

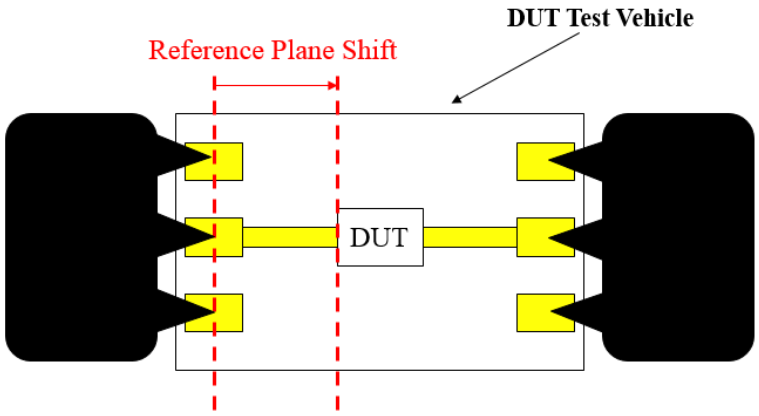

Figure 1.2: Example Location of Reference Plane After De-embedding

correction. Calibration first moves the reference plane to some location on the DUT test vehicle by removing the parasitic effects induced from cables, adapters, probes, and parasitics internal to the VNA. De-embedding is then performed, completing the shift of the reference plane up to the DUT by removing the unwanted effects of test fixtures.

1.2 MOTIVATION

1.2.1 The Need for De-embedding Advancement. As described previously, de-embedding is needed to complete the shift of the reference plane up to the DUT. In other words, de-embedding allows for the complete extraction of the electrical performance of the DUT. At the printed circuit board level, de-embedding techniques are very mature and highly accurate. De-embedding techniques at the silicon level are far less mature.

As semiconductor structures continue to shrink to ever smaller sizes, extracting the electrical performance of these structures (on-wafer device characterization), through de-embedding, is becoming increasingly more difficult. The more the structures shrink in size, the more easily their electrical performance is overshadowed by other, larger structures. Advanced devices enable advanced designs, but advanced designs depend on highly accurate measurements for device characterization, so de-embedding must inevitably advance as well.

1.2.2 Limitations of De-embedding at the Silicon Level. Currently, three major drawbacks limit de-embedding techniques employed at the silicon level. First, inaccurate models of silicon fixtures limit the accuracy of the DUT extraction. Second, many techniques require too much silicon area for structures required for de-embedding. Finally, the approach taken for validating many of the current de-embedding techniques is not intuitive and is not complete.

1.2.3 De-embedding Application to TSVs. State-of-the-art de-embedding techniques at the silicon level almost exclusively examine transmission lines. A new silicon structure for application with 3D integrated circuits (ICs) is

the through-silicon-via (TSV). The electrical performance of TSVs is not yet fully understood, but is essential for designing the next generation of IC systems.

1.3 OBJECTIVES

In this thesis, state-of-the-art de-embedding techniques at the silicon level are thoroughly investigated. Following the investigation, new formulations are explored for de-embedding silicon structures. After the exploration of new formulations, an evaluation is performed to determine the best method (or combination of methods) for de-embedding silicon transmission lines and TSVs. The ability to extract the performance of transmission lines is highly important as transmission lines are a fundamental interconnect structure for ensuring signal integrity in high-speed designs. The ability to extract the electrical performance of TSVs is essential for advanced IC designs and to formulate a complete physical understanding of the TSV structure.

1.4 CONTRIBUTIONS

Several contributions are made towards advancements in device measurement and characterization, including the following:

- A more intuitive approach to verifying the accuracy of de-embedding techniques using scattering parameters.
- A complete evaluation of several de-embedding techniques (including attempts at new formulations), leading to the selection of a best choice technique for de-embedding TSVs.

The results of the research for this thesis have resulted in one conference publication, as given in [2].

1.5 OUTLINE

The remainder of this thesis is organized as follows: Section 2 presents a review of literature describing current, state-of-the-art de-embedding techniques; Section 3 describes the approach used in this thesis to evaluate de-embedding techniques, along with attempts at formulating new de-embedding techniques; Section 4 interprets the results of Section 3 to arrive at a best choice technique for de-embedding TSVs; and Section 5 describes the implications of, and outlines a course for further extensions to, this thesis' work.

2. BACKGROUND AND RELATED WORK

2.1 TWO IMPEDANCE THROUGH METHOD

The core of many of the surveyed de-embedding techniques rely on the two impedance through model to solve for the parasitics created by the on-wafer pad structures. Therefore, the two impedance through method, as given by Song et al. in [1], is summarized first.

The method states that if adapters (or pad structures, in the case of on-wafer measurements) are modeled with three unknowns, only two equations can be generated. The three unknowns represent the reflections looking in from each side of the adapter, along with the transmission of the adapter. Symmetry is assumed, with one adapter representing a mirror of the other adapter. The model for the adapters is shown in Equation 2.1, where the superscript 'L' denotes the left pad. Since the right pad is considered a mirror of the left pad, it can be represented in terms of the left pad.

$$S_{Left} = \begin{bmatrix} S_{11}^{L} & S_{12}^{L} \\ S_{12}^{L} & S_{22}^{L} \end{bmatrix} \qquad S_{Right} = \begin{bmatrix} S_{22}^{L} & S_{12}^{L} \\ S_{12}^{L} & S_{11}^{L} \end{bmatrix} \tag{2.1}$$

The two generated equations that arise from the through measurement are shown in Equations 2.2 and 2.3. Again, the 'L' superscript indicates characteristics for the left pad. The "through" superscript indicates characteristics for the total through structure, i.e. a cascade of the left pad with the right pad.

$$S_{11}^{Through} = S_{11}^{L} + S_{12}^{Through} S_{22}^{L} \tag{2.2}$$

$$(S_{12}^{L})^2 = (1 - (S_{22}^{L})^2) S_{12}^{Through} \tag{2.3}$$

To avoid equating the reflections (since most adapters do not have a symmetric left and right half), the two impedance through model is given in Figure 2.1. This

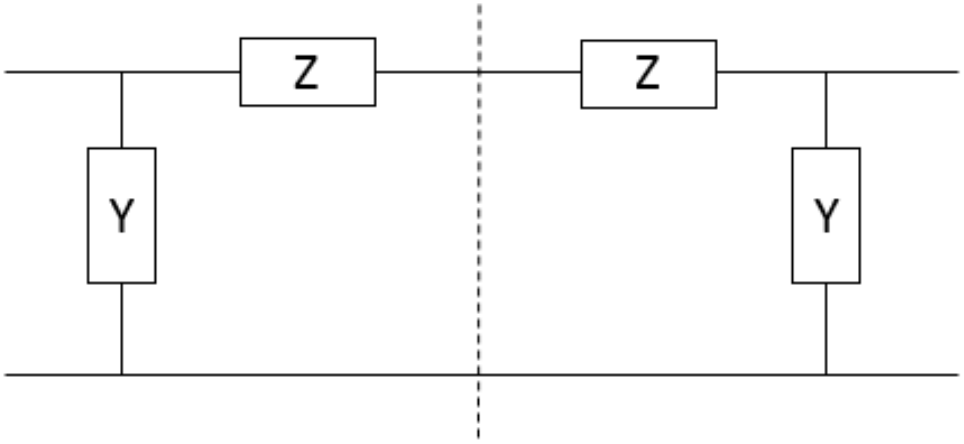

Figure 2.1: 2-Impedance Model of Through [1]

model avoids the requirement of having adapters with symmetric planes, while still reducing the number of unknown pad parameters to two. Utilizing Z-parameter and Y-parameter 2-port circuit definitions, the unknown shunt admittance (Y) and the unknown series impedance (Z) can be solved for, resulting in Equations 2.4 and 2.5.

$$Z = \frac{-1}{2Y_{12}^{Through}} \tag{2.4}$$

$$Y = Y_{11}^{Through} + Y_{12}^{Through} \tag{2.5}$$

With Z and Y known, the adapters can be characterized into any of the respective network parameter sets. The adapters can then be removed from a total DUT measurement. However, most measurements are not simply the DUT connected with an adapter on either end; usually, some length of interconnect exists between the

adapters and the DUT. Section 2.2 and Section 2.3 describe techniques capable of de-embedding both adapters and interconnects from DUTs.

2.2 L-2L METHOD

Building upon the 2-Impedance Through Method, the L-2L Method, as proposed by Li et al. in [3], can additionally handle adapters including some length of interconnect. No through is ever measured in this method; instead, a through is synthesized from the measurement of an L length transmission line (including pads) and a 2L length transmission line (also including pads). The representations of the two transmission lines (in terms of ABCD parameters) are given in Equations 2.6 and 2.7, where the subscript "Tx" stands for "transmission line" and the superscript "Tot" indicates the total cascaded system (pads+transmission line).

$$ABCD_{TxL}^{Tot} = ABCD_{PadL}ABCD_{TxL}ABCD_{PadR} \tag{2.6}$$

$$ABCD_{Tx2L}^{Tot} = ABCD_{PadL}ABCD_{Tx2L}ABCD_{PadR} \tag{2.7}$$

To synthesize the through, the total measurement for the 2L line (Equation 2.7) is inverted and then left and right multiplied by the total measurement for the L line (Equation 2.6), resulting in a through of the pads (Equations 2.8 and 2.9). The pads can be solved using the 2-Impedance Model given in Section 2.1 if the right pad is considered a mirror of the left pad.

$$ABCD_{Thru} = ABCD_{TxL}^{Tot}(ABCD_{Tx2L}^{Tot})^{-1}ABCD_{TxL}^{Tot} \tag{2.8}$$

$$= ABCD_{PadL}ABCD_{PadR} \tag{2.9}$$

After solving for the pads, they can be inverted and left and right multiplied on the total measurements for the L and 2L length line (Equations 2.6 and 2.7),

leaving only the true lines. In the case where the transmission line is the DUT, the de-embedding procedure is complete.

This technique can further be applied for other DUTs if the DUTs utilize a length of transmission line as an interconnect between themselves and the pad structures. For example, if an arbitrary DUT is embedded in the center of the total 2L length transmission line structure, then two modified adapters can be constructed. The modified left adapter is the right multiplication of the solved left pad by the solved L length transmission line. The modified right adapter is the left multiplication of the solved right pad by the solved L length of transmission line. By left and right multiplying the total DUT measurement by inverted versions of the modified adapters, the DUT can be fully de-embedded.

2.3 LILJ METHOD

Similar to the L-2L method, the LiLj method, proposed by Mangan et al. in [4], requires two transmission line structures to de-embed the true transmission lines. In this method, however, one line is not required to be double the length of the other; instead, the lines are only required to be two different lengths. The two line representations (in terms of ABCD parameters) are given in Equations 2.10 and 2.11, where the subscript "Li" represents a transmission line of length i and the superscript "Tot" denotes the total structure (transmission lines+pads).

$$ABCD_{Li}^{Tot} = ABCD_{PadL}ABCD_{Li}ABCD_{PadR} \tag{2.10}$$

$$ABCD_{Lj}^{Tot} = ABCD_{PadL}ABCD_{Lj}ABCD_{PadR} \tag{2.11}$$

Inverting the shorter line (Li), followed by a left multiplication of the longer line (Lj), results in a hybrid line of length Lj-Li. As shown in Equation 2.12, the hybrid line

no longer involves the right pad, but does involve an inverted form of the left pad.

$$ABCD_{Lj-Li}^{Hybrid} = ABCD_{PadL}ABCD_{Lj-Li}(ABCD_{PadL})^{-1} \tag{2.12}$$

Instead of using two lumped elements for the pad structure, this method only assumes the pad is a single lumped admittance. By converting the total hybrid line network in Equation 2.12 to Y parameters, the pads can simply be added to the total network if they are considered to be in parallel with the transmission lines. Adding the hybrid line with a port swapped version of itself (indicated by "Swap()" in Equation 2.14), and then dividing by 2, one can find that the effect of the pads are canceled, leaving only the hybrid length line. This process is illustrated in Equations 2.13 and 2.14, where the superscript "Hybrid" indicates the hybrid length line including the effect of the pads, the 'Y' with the subscript "Pad" represents the lumped admittance for the pad, and the 'Y' with the subscript "Lj-Li" indicates the Y-parameter representation of a line with length Lj-Li.

$$Y_{Li-Lj}^{Hybrid} = Y_{Li-Lj} + \begin{bmatrix} Y_{Pad} & 0 \\ 0 & -Y_{Pad} \end{bmatrix} \tag{2.13}$$

$$Y_{Li-Lj} = \frac{Y_{Li-Lj}^{Hybrid} + Swap(Y_{Li-Lj}^{Hybrid})}{2} \tag{2.14}$$

2.4 TSD CALIBRATION

A final error correcting technique worth describing is the original through-short-delay (TSD) method presented by Franzen and Speciale in [5]. In this method, three reference standards are required as indicated by the method's name: a through, a short, and a delay. The total system, including the DUT, can be represented as cascade of scattering matrices as shown in Equation 2.15. Here, the superscript "Tot"

refers to the total cascaded system, the '$*$' denotes the cascade procedure, and the superscripts 'A' and 'B' indicate the left and right error networks, respectively.

$$S_{DUT}^{Tot} = S_{Error}^{A} * S_{DUT} * S_{Error}^{B} \tag{2.15}$$

Inserting each reference standard in place of the DUT, Equations 2.16 - 2.18 can be obtained.

$$S_{Thru}^{Tot} = S_{Error}^{A} * S_{Error}^{B} \tag{2.16}$$

$$S_{Short}^{Tot} = S_{Error}^{A} * S_{Short} * S_{Error}^{B} \tag{2.17}$$

$$S_{Delay}^{Tot} = S_{Error}^{A} * S_{Delay} * S_{Error}^{B} \tag{2.18}$$

If the error boxes are considered different and if they are each considered reciprocal, then each error box contains three unknowns. So the two error boxes represent six complex unknowns. Equation 2.16 gives three equations. Equation 2.17 only gives two equations because no transmission occurs, thus $S_{12} = S_{21} = 0$ for the total short system. However, an additional unknown for the reflection is also introduced. Finally, Equation 2.18 introduces an additional unknown for the delay line, but three additional equations. In total, there are eight complex unknowns with eight complex equations, allowing all unknowns to be solved.

After solving for all the unknowns, error box A and error box B can be fully characterized. Using ABCD or T parameters, the error box matrices can be inverted and then left and right multiplied on Equation 2.15, resulting in the matrix for the true DUT. It must be noted that this procedure assumes a delay line with a characteristic impedance that exactly matches the reference impedance of the system. In this way, the delay line does not include a component for reflections, eliminating the need for an additional unknown.

3. APPROACH

3.1 OUTLINE

This section will first attempt to formulate two new techniques for de-embedding silicon structures. Following the formulation, the process used for evaluating the various de-embedding techniques is described. The results of the evaluation process are presented in Section 4, leading to best choice de-embedding technique for TSVs.

3.2 FORMULATION ATTEMPT I: HYBRID METHOD

3.2.1 Introduction to Attempt I. Drawing from the L-2L [3] and LiLj [4] de-embedding techniques previously discussed in Section 2, the first attempt at a new de-embedding technique focused on lumped elements for the pad structures. The so called Hybrid method requires two transmission line structures: one of length L, and one of length 2L. Elements of both the L-2L and LiLj formulations are utilized in this method.

3.2.2 Adapter Structure. Observing the pad structures used in the 2-Impedance Through Method [1] and the L-2L method [3], as shown in Figure 2.1, the series impedance is placed after the shunt admittance. By swapping this ordering, the model better approaches the reality of probing measurements: the resistance of the pad is encountered first as the signal travels towards the transmission line, followed by a capacitance formed by the multi-metal layered pad structure. The swapped model is given in Figure 3.1.

3.2.3 Removing the Z Portion of the Pads. Utilizing the L-2L method [3], a through of the adapters is obtained by first inverting the 2L line, followed by a left and right multiplication of the L line. Here the equation for the

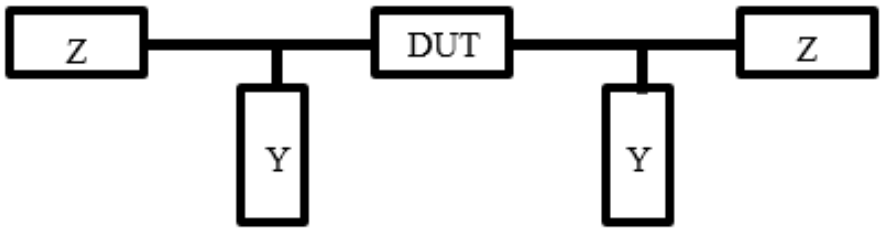

Figure 3.1: Swapped Impedance Pad Model

series impedance (Z) is re-derived, in terms of Z parameters, to account for the swap in the adapter structure. An ABCD network is then built for Z. Since Z appears on the outside of the total transmission line structures, the Z network can be inverted and then removed the total structures. The process is shown in Equations 3.1 - 3.4, where 'Z' (without a subscript) represents the series impedance, 'Z' with the subscript "thru" represents the through of the pads in terms of Z parameters, the superscript "Tot" indicates the line with the effect of the pads, the subscript 'L' represents the length of the line, and the subscript "LnoZ" indicates a line (of length L) including pads, just with the Z portion of the pads removed.

$$Z = Z_{thru}(1,1) - Z_{thru}(1,2) \tag{3.1}$$

$$ABCD_Z = \begin{bmatrix} 1 & Z \\ 0 & 1 \end{bmatrix} \tag{3.2}$$

$$ABCD_{2LnoZ} = ABCD_Z^{-1} ABCD_{2L}^{Tot} ABCD_Z^{-1} \tag{3.3}$$

$$ABCD_{LnoZ} = ABCD_Z^{-1} ABCD_{L}^{Tot} ABCD_Z^{-1} \tag{3.4}$$

3.2.4 Removing the Y Portion of the Pads. After removing the Z portion of the pads, only the Y portion remains. This model fits the model given by the LiLj method [4], so that procedure is repeated to remove the Y portion of

the pads. The result is a de-embedded hybrid line of length 2L-L = L. The process is shown in Equations 3.5 and 3.6, where all subscripts/superscripts have the same meaning as previously described in Section 2.3.

$$Y_{2L-L}^{Hybrid} = Y_{2L-L} + \begin{bmatrix} Y_{Pad} & 0 \\ 0 & -Y_{Pad} \end{bmatrix} \tag{3.5}$$

$$Y_{2L-L} = \frac{Y_{2L-L}^{Hybrid} + Swap(Y_{2L-L}^{Hybrid})}{2} \tag{3.6}$$

3.2.5 Comments on Attempt I. The Hybrid method attempts to improve the L-2L [3] method by modeling the pad structure so that the contact resistance created by the landing of micro-probes on the pad is encapsulated into the series impedance that is swapped to the outside of the pad. In addition, a more complete pad model is offered (series impedance and shunt admittance) compared to the single lumped pad model offered by the LiLj [4] method.

3.3 FORMULATION ATTEMPT II: NON-LUMPED L-2L METHOD

3.3.1 Introduction to Attempt II. All de-embedding methods based on simple lumped elements lack generality in describing arbitrary pad structures. Compared to standard calibration techniques that employ "error networks" to describe measurement parasitics, lumped element techniques also lack in mathematical rigor. The formulation that is attempted below was inspired by the through-short-delay (TSD) calibration, a formulation that is both general and mathematically rigorous.

3.3.2 Transmission Line Structure. Consider an on-wafer transmission line. Using s-parameters, the transmission line can be represented as a cascade of three network blocks: a block for the left pad, a block for the transmission line, and a block for the right pad.

For the most general case, each network block would contain four complex unknowns, totaling twelve complex unknowns in all. Three of the unknowns (one insertion loss term per network) are easily discarded, however, as all components of the transmission line structure are considered reciprocal, i.e. $S_{12} = S_{21}$. Additionally, three more unknowns vanish if the right pad structure is considered a mirror of the left pad structure. Finally, two more unknowns (the return losses of the transmission line) drop away if the transmission line is considered to be in a perfectly matched state. Therefore, the unknowns can reduce from twelve down to four, in the case of the observed transmission line structure. The new representation of the total transmission line network is shown in Equation 3.7, where the superscript 'L' denotes the left pad, "$e^{\gamma l}$" denotes the delay of a line of length l, and the subscript "Tot" indicates the total cascade of the system. Again, '$*$' indicates the cascading process.

$$S_{Tot} = \begin{bmatrix} S_{11}^L & S_{12}^L \\ S_{12}^L & S_{22}^L \end{bmatrix} * \begin{bmatrix} 0 & e^{\gamma l} \\ e^{\gamma l} & 0 \end{bmatrix} * \begin{bmatrix} S_{22}^L & S_{12}^L \\ S_{12}^L & S_{11}^L \end{bmatrix} \tag{3.7}$$

3.3.3 Formulation Issue: Matched Transmission Line. Using this representation of the transmission line structure, the number of unknowns is greatly reduced without any real loss in generality. Here an important point must be noted with the formulation: the network representation of the transmission line assumes the matched case. For the matched case, all s-parameter network blocks must be referenced to the characteristic impedance, Z_o, of the transmission line. For a perfect 50 ohm transmission line, no problem arises, as most network analyzers present a 50 ohm reference impedance. The TSD method uses this exact assumption in the case of its delay line measurement; the delay line is required to be 50 ohms so that the line does not produce any reflections. In this case, the four unknowns can be solved with the four available equations. In reality, fabricated transmission lines will not have a perfectly frequency invariant characteristic impedance, especially at the silicon level.

Even at frequencies where the characteristic impedance does not vary, it is unlikely to match the target impedance precisely.

Considering reality, not only will the characteristic impedance of the transmission line not be exactly 50 ohms, it will not be known. Here another interesting problem, unique to silicon structures, arises. For printed circuit board (PCB) structures, time domain techniques, namely time domain reflectometry (TDR), could determine the characteristic impedance of the transmission line. The automatic fixture removal (AFR) method developed by Agilent Technologies takes advantage of TDR to aid in de-embedding measurement fixtures from DUTs. Since PCB structures generally have sizes on the order of millimeters or centimeters, they are easily resolved with TDR rise times on the order of 25 or more picoseconds. TDRs with such rise times exist.

For silicon structures, TDR cannot be employed because the structures are simply too small. To resolve ultra small silicon structures, i.e. pad structures, the required TDR rise time approaches 1 picosecond; current technology cannot realize rise times on this order. The same restriction is found with TDR responses created from frequency domain content; to realize a 1 picosecond rise time, frequency content out to and past 800 GHz would be required.

3.3.4 Realizing the Matched Transmission Line. So one reasonable approach is to generate an equivalent 50 ohm transmission line. Interestingly, a transmission line, no matter its characteristic impedance, can be transformed into a transmission line of another characteristic impedance, as stated by Bianco et al. in [6]. By observing the total structure in terms of ABCD network parameters, it can be proved that, with the addition of some ideal transformers, the effects of the non-50 ohm transmission line can be absorbed into the pad structures. After the transformers are added, the total system resembles the delay line measurement in the TSD calibration method, as presented in Section 2.4. The proof for the impedance transform

is quickly derived below. In the equations below, the subscript "Tfmr" represents the network for a transformer, 'n' represents the scaling factor of the transformer, "Z_o" represents the characteristic impedance of a transmission line, and the subscript "Tx" represents the network for a transmission line with characteristic impedance of "Z_o". ABCD Parameters for Left and Right Pad Structures:

$$ABCD_{PadL} = \begin{bmatrix} A & B \\ C & D \end{bmatrix} \qquad ABCD_{PadR} = \begin{bmatrix} D & B \\ C & A \end{bmatrix} \tag{3.8}$$

ABCD Parameters for Ideal n:1 Transformer and Ideal 1:n Transformer:

$$ABCD_{Tfmr1} = \begin{bmatrix} n & 0 \\ 0 & 1/n \end{bmatrix} \qquad ABCD_{Tfmr2} = \begin{bmatrix} 1/n & 0 \\ 0 & n \end{bmatrix} \tag{3.9}$$

ABCD Parameters for Transmission Line with Arbitrary Zo:

$$ABCD_{Tx} = \begin{bmatrix} \cosh(\gamma l) & Z_o \sinh(\gamma l) \\ \frac{1}{Z_o}\sinh(\gamma l) & \cosh(\gamma l) \end{bmatrix} \tag{3.10}$$

Total ABCD Network for Pad-Transformer-Equivalent Transmission Line Structure:

$$\begin{bmatrix} A & B \\ C & D \end{bmatrix} \begin{bmatrix} n & 0 \\ 0 & 1/n \end{bmatrix} \begin{bmatrix} \cosh(\gamma l) & 50\sinh(\gamma l) \\ \frac{1}{50}\sinh(\gamma l) & \cosh(\gamma l) \end{bmatrix} \begin{bmatrix} 1/n & 0 \\ 0 & n \end{bmatrix} \begin{bmatrix} D & B \\ C & A \end{bmatrix} \tag{3.11}$$

The multiplication of the middle three sections of Equation 3.11 then yields the result in Equation 3.12:

$$\begin{bmatrix} \cosh(\gamma l) & 50n^2\sinh(\gamma l) \\ \frac{1}{50n^2}\sinh(\gamma l) & \cosh(\gamma l) \end{bmatrix} \tag{3.12}$$

Letting $n^2 = \frac{Z_o}{50}$, Equation 3.12 becomes the original transmission line matrix given in Equation 3.10, proving that the original transmission line can be treated as a transmission line with a 50 ohm impedance, in conjunction with two ideal transformers.

Re-observing Equation 3.11, the transformer effects can be absorbed into the left and right pads, as given in Equation 3.13. Noticing that the right pad is still a mirror of the left pad after absorbing the effects of the transformers, the total, modified transmission line structure can be represented as in Equation 3.14, when converted from ABCD parameters to scattering parameters (with all ports referenced to 50 ohms). In Equation 3.14, '$*$' indicates the cascade procedure, the superscript 'L'' indicates the modified left pad, and the subscript "ModTot" represents the total cascade of the modified structure.

$$ABCD_{ModTot} = \begin{bmatrix} nA & \frac{1}{n}B \\ nC & \frac{1}{n}D \end{bmatrix} \begin{bmatrix} \cosh(\gamma l) & Z_o \sinh(\gamma l) \\ \frac{1}{Z_o}\sinh(\gamma l) & \cosh(\gamma l) \end{bmatrix} \begin{bmatrix} \frac{1}{n}D & \frac{1}{n}B \\ nC & nA \end{bmatrix} \tag{3.13}$$

$$S_{ModTot} = \begin{bmatrix} S_{11}^{L'} & S_{12}^{L'} \\ S_{12}^{L'} & S_{22}^{L'} \end{bmatrix} * \begin{bmatrix} 0 & e^{\gamma l} \\ e^{\gamma l} & 0 \end{bmatrix} * \begin{bmatrix} S_{22}^{L'} & S_{12}^{L'} \\ S_{12}^{L'} & S_{11}^{L'} \end{bmatrix} \tag{3.14}$$

Comparing Equation 3.14 to Equation 3.7, the two systems are the same, in terms of form and the number of unknowns. Using two transmission lines with the modified form, one of length L and one of length 2L, four equations are generated, allowing the four unknowns to be solved.

3.3.5 Formulation of Transmission Line Half Structures. Using the form developed in 3.3.4 for a transmission line of length L and a transmission line of length 2L, the networks shown in Equation 3.15 can be formed, where all subscripts

and superscripts retain the same meanings as described in previous sections.

$$S_{T1} = \begin{bmatrix} S_{11}^{L'} & S_{12}^{L'} \\ S_{12}^{L'} & S_{22}^{L'} \end{bmatrix} * \begin{bmatrix} 0 & e^{-\gamma l} \\ e^{-\gamma l} & 0 \end{bmatrix} * \begin{bmatrix} S_{22}^{L'} & S_{12}^{L'} \\ S_{12}^{L'} & S_{11}^{L'} \end{bmatrix} \tag{3.15}$$

$$S_{T2} = \begin{bmatrix} S_{11}^{L'} & S_{12}^{L'} \\ S_{12}^{L'} & S_{22}^{L'} \end{bmatrix} * \begin{bmatrix} 0 & e^{-2\gamma l} \\ e^{-2\gamma l} & 0 \end{bmatrix} * \begin{bmatrix} S_{22}^{L'} & S_{12}^{L'} \\ S_{12}^{L'} & S_{11}^{L'} \end{bmatrix} \tag{3.16}$$

Using the cascading procedure for three, two-port s-parameter blocks, Equations 3.17-3.20 are generated, where S_{11}^{T1} represents the return loss for an L length, 50 ohm transmission line with pads; S_{11}^{T2} represents the return loss for a 2L length, 50 ohm transmission line with pads; S_{12}^{T1} represents the insertion loss for an L length, 50 ohm transmission line with pads; and, S_{12}^{T1} represents the insertion loss for a 2L length, 50 ohm transmission line with pads. Additionally, the superscript "T1" stands for the total cascade of an L length line with pads. The superscript "T2" stands for the total cascade of a 2L length line with pads.

$$S_{11}^{T1} = S_{11}^{L'} + \frac{(S_{12}^{L'})^2 e^{-2\gamma l} S_{22}^{L'}}{1 - (S_{22}^{L'})^2 e^{-2\gamma l}} \tag{3.17}$$

$$S_{11}^{T2} = S_{11}^{L'} + \frac{(S_{12}^{L'})^2 e^{-4\gamma l} S_{22}^{L'}}{1 - (S_{22}^{L'})^2 e^{-4\gamma l}} \tag{3.18}$$

$$S_{12}^{T1} = \frac{(S_{12}^{L'})^2 e^{-\gamma l}}{1 - (S_{22}^{L'})^2 e^{-2\gamma l}} \tag{3.19}$$

$$S_{12}^{T2} = \frac{(S_{12}^{L'})^2 e^{-2\gamma l}}{1 - (S_{22}^{L'})^2 e^{-4\gamma l}} \tag{3.20}$$

To solve the equations, MATLAB's symbolic equation solver was used. The results of the solved equations are complex and lengthy, so they are not presented here. With all unknowns solved, the left and right transmission line half structures can be constructed as in Equations 3.21 and 3.22, where the subscript "LH" means

the left half (and the subscript "RH" means the right half) of the transmission line structure.

$$S_{LH} = \begin{bmatrix} S_{11}^{L'} & S_{12}^{L'} \\ S_{12}^{L'} & S_{22}^{L'} \end{bmatrix} * \begin{bmatrix} 0 & e^{-\gamma l} \\ e^{-\gamma l} & 0 \end{bmatrix} \tag{3.21}$$

$$S_{RH} = \begin{bmatrix} 0 & e^{-\gamma l} \\ e^{-\gamma l} & 0 \end{bmatrix} * \begin{bmatrix} S_{22}^{L'} & S_{12}^{L'} \\ S_{12}^{L'} & S_{11}^{L'} \end{bmatrix} \tag{3.22}$$

3.3.6 Comments on Attempt II. At first glance the results in Section 3.3.5 would appear to be a rather elegant solution for de-embedding. However, upon further inspection, the formulation has a pitfall. Take for example the case where the DUT to be de-embedded is just another transmission line of length L. The total structure can be described in terms of ABCD parameters as in Equation 3.23. For readability, 'M' is used as an alternate representation of an ABCD matrix in Equation 3.23. Additionally, the superscript "50" indicates a transmission line with a characteristic impedance of 50 ohms and the subscript "TxL" represents a transmission line of length L.

$$M_{3L}^{Tot} = M_{PadL} M_{Tfmr1} M_{TxL}^{50} M_{Tfmr2} M_{Tfmr1} M_{TxL}^{50} M_{Tfmr2} M_{Tfmr1} M_{TxL}^{50} M_{Tfmr2} M_{PadR} \tag{3.23}$$

Referencing Section 3.3.4, the solved halves of the L transmission line structure (Equations 3.21 and 3.22) can be represented in terms of ABCD parameters. Those representations are given below in Equations 3.24 and 3.25.

$$M_{LH} = M_{PadL} M_{Trfm1} M_{TxL}^{50} \tag{3.24}$$

$$M_{RH} = M_{TxL}^{50} M_{Trfm2} M_{PadR} \tag{3.25}$$

Performing the typical inverse/multiply to remove the right and left halves from Equation 3.23, leaves Equation 3.26, where the superscript "Tot" represents a total line including the effect of pads.

$$M_{LH}^{-1} M_{3L}^{Tot} M_{RH}^{-1} = M_{Tfmr2} M_{Tfmr1} M_{TxL}^{50} M_{Tfmr2} M_{Tfmr1} \tag{3.26}$$

$$= M_{TxL}^{50} \tag{3.27}$$

The multiplication of transformer 1 by transformer 2 decomposes to the identity matrix leaving only the L length transmission line (DUT), with the non-50 ohm scaling factor removed (Equation 3.27). This means the de-embedded result is not the true DUT.

One solution for this pitfall could be to use transformers (or the non-50 ohm scaling factor) to get back to the true DUT performance, but this requires knowledge of characteristic impedance of the original L and 2L lines. Without knowing Zo, though, this approach cannot be applied appropriately. For silicon structures, Zo is likely to be unknown, as discussed in Section 3.3.3. Thinking again in terms of equations and unknowns, Zo adds a fifth unknown. Shorts, opens, loads, and other lines cannot generate a fifth equation, so the system remains under-determined. The same constraints found with this formulation attempt appear in the formulation of the TSD calibration procedure, as discussed in Section 2.4.

3.4 THE THROUGH: REVISITED

One final thought is given to non-lumped de-embedding techniques. By again observing the through described in [1] and Section 2.1, 3 unknowns with only 2 equations exist before the 2-Impedance approximation. The 2-Impedance model is used to avoid equating the reflections looking into each port of the adapter. What if letting $S_{11}^{L} = S_{22}^{L}$ is not a bad approximation since the pad structures, though not

symmetric physically, are so small that they are approximately symmetric electrically? Such an assumption reduces the number of unknowns to two, allowing the unknowns to be solved, resulting in Equations 3.28 and 3.29:

$$S_{11}^{L} = \frac{S_{11}^{Through}}{1 + S_{12}^{Through}} \tag{3.28}$$

$$S_{12}^{L} = \pm\sqrt{S_{12}^{Through}(1 - (S_{11}^{L})^2)} \tag{3.29}$$

The validity of the $S_{11}^{L} = S_{22}^{L}$ claim is discussed in Section 4. As a note, one need not have an actual through available for measurement if the L-2L technique is used to arrive at the through condition.

3.5 EVALUATION APPROACH: MODELS AND MEASUREMENTS

To evaluate the discussed de-embedding techniques, both simulations and actual measurements are used. Simulations include full-wave models in Ansys' HFSS and some analytic models in Agilent's ADS. An IC including transmission lines of length 100um, 1000um, and 2000um was manufactured for use in evaluating the de-embedding techniques for transmission lines (L-2L, LiLj, and Through) as well. The steps for evaluation are as follows:

- Verify De-embedding Methods with Simulations
- Verify De-embedding Methods with Measurements (if possible)
- Compare Simulations and Measurements
- Compare Results Between Methods

For the end evaluation, the main influencing factors are level of reasonableness and consistency between simulations and measurements. Using these factors, the most robust method can be chosen for application in de-embedding TSVs.

As opposed to many of the methods in literature, the work in this thesis uses scattering parameters for all verification procedures. This approach is more intuitive than verification through transmission line characteristics because real measurements are given in terms of scattering parameters. Additionally, scattering parameters easily describe non-transmission line structures; for example, if characterizing the adapter is also important, describing the adapter in terms of transmission line characteristics does not make sense. The value of this approach is investigated in Section 4.

4. EVALUATION

4.1 SIMULATION VERIFICATION OF LUMPED METHODS

A single set of full-wave models was used for verifying all the lumped models so that a fair comparison could be made between the methods. Although not practical for actual measurements, a stripline was chosen for modeling due to its simplicity and ease of simulation. A simple "block" pad was placed on the ends of the stripline to emulate a discontinuity to be removed. The model was then simulated up to 50GHz in Ansys' HFSS. The model is given in Figure 4.1.

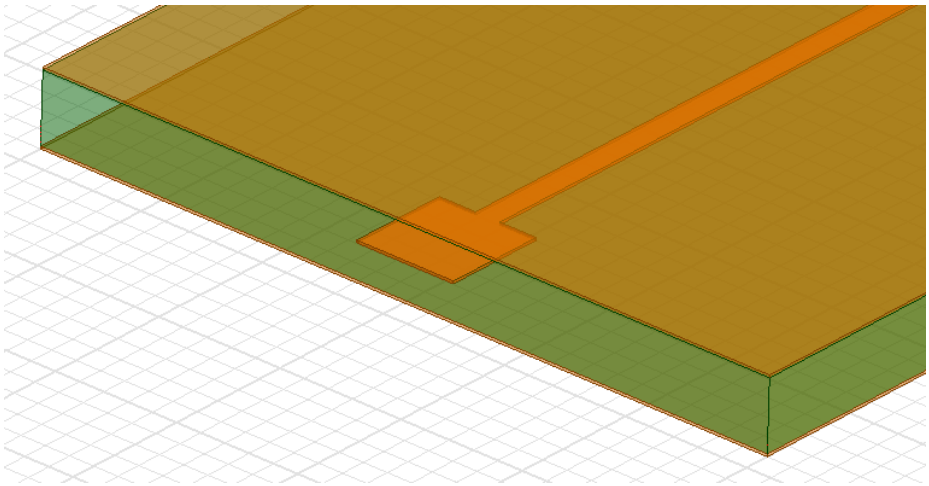

Figure 4.1: Stripline + Pad Model in HFSS

Although all results are given in [2], they are quickly summarized here. The first case is for the L-2L method, where L=900um and 2L=1800um. After de-embedding, the ideal 2L=1800um line is presented in Figures 4.2 and 4.3. Next the results of the LiLj method are presented for a de-embedded Lj-Li=900um line in Figures 4.4 and 4.5,where the original lines were Li=900um and Lj=1800um. Finally,

a de-embedded line of length 2L-Li=1900 is presented for the hybrid method in Figures 4.6 and 4.7. The initial lines for this simulation were 2L=2000um, L=1000um, and Li=100um.

From the simulation results, all methods were found to work suitably well up to 50GHz. As discussed in [2], the only method that showed some restriction was the LiLj method for when the series impedance began to significantly dominate over the shunt capacitance.

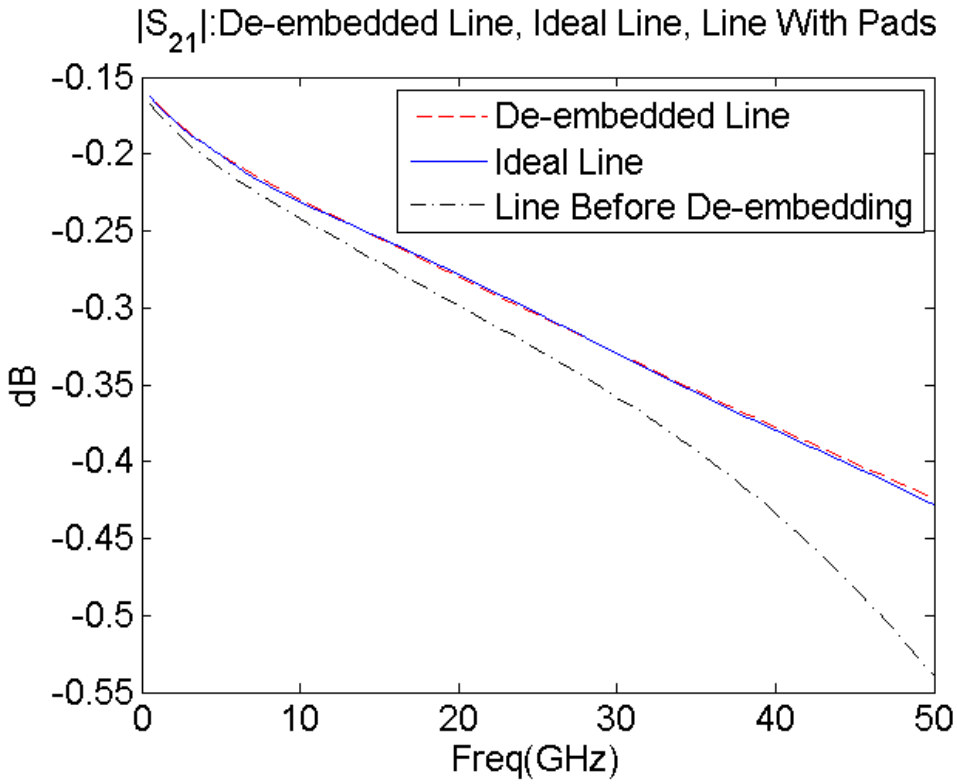

Figure 4.2: L-2L De-embedding Results for 2L=1800um (S_{21})

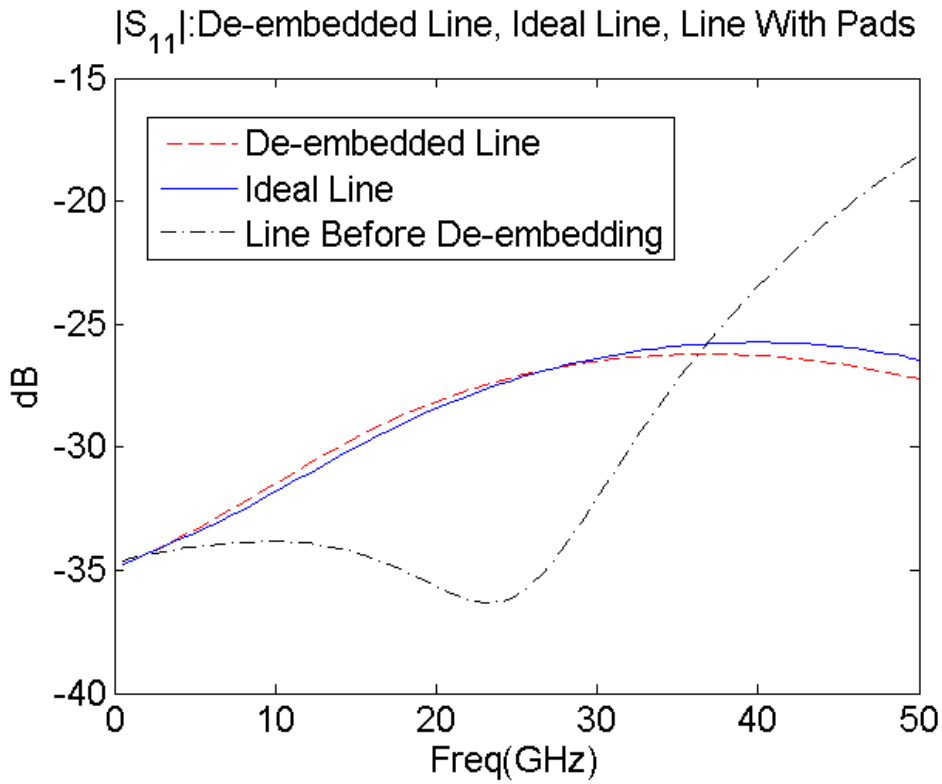

Figure 4.3: L-2L De-embedding Results for 2L=1800um (S_{11})

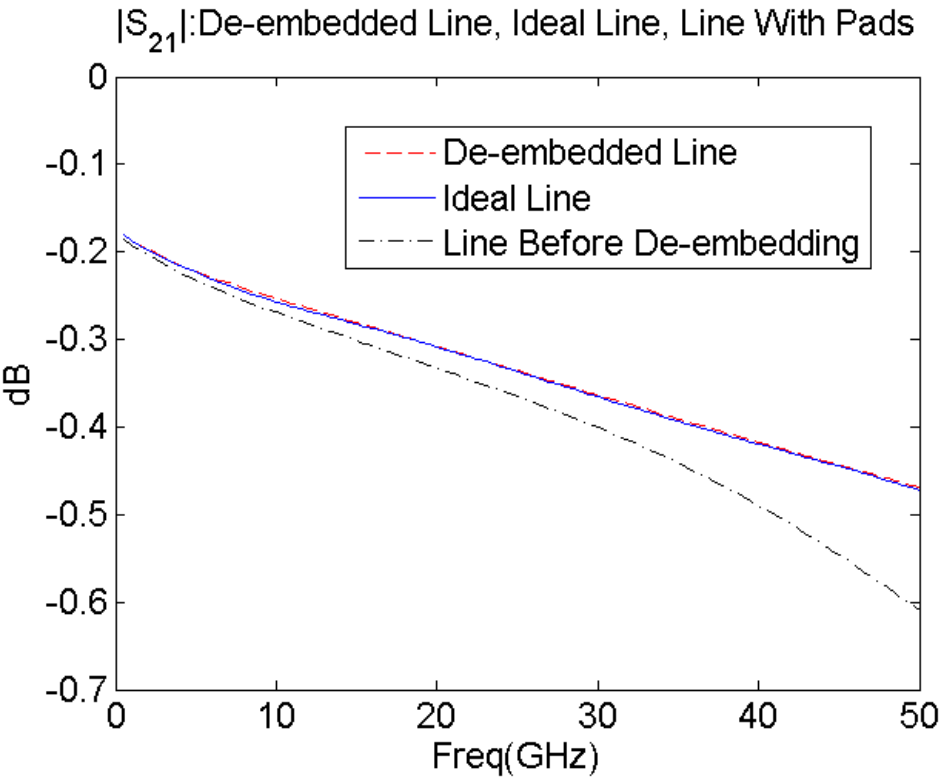

Figure 4.4: LiLj De-embedding Results for Lj-Li=900um (S_{21})

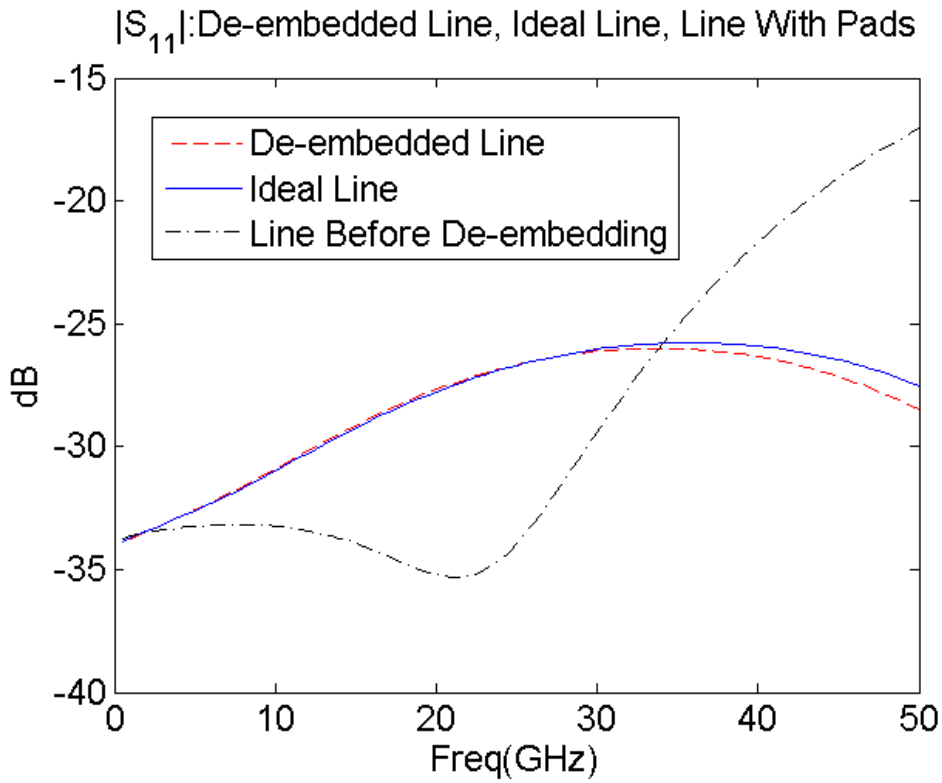

Figure 4.5: LiLj De-embedding Results for Lj-Li=900um (S_{11})

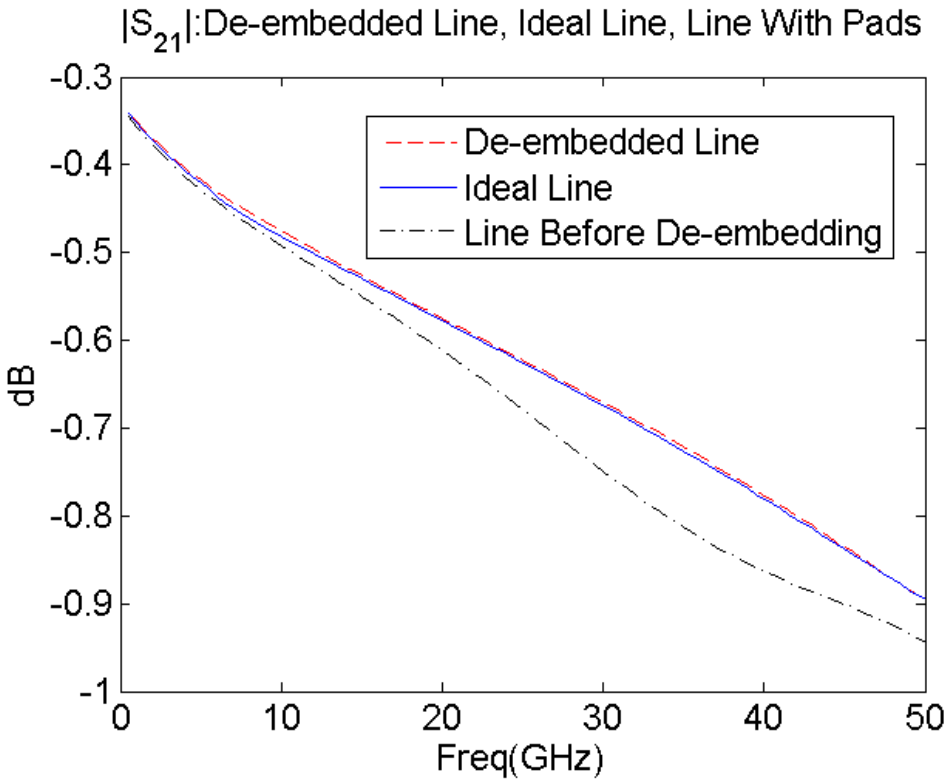

Figure 4.6: Hybrid De-embedding Results for 2L-Li=1900um (S_{21})

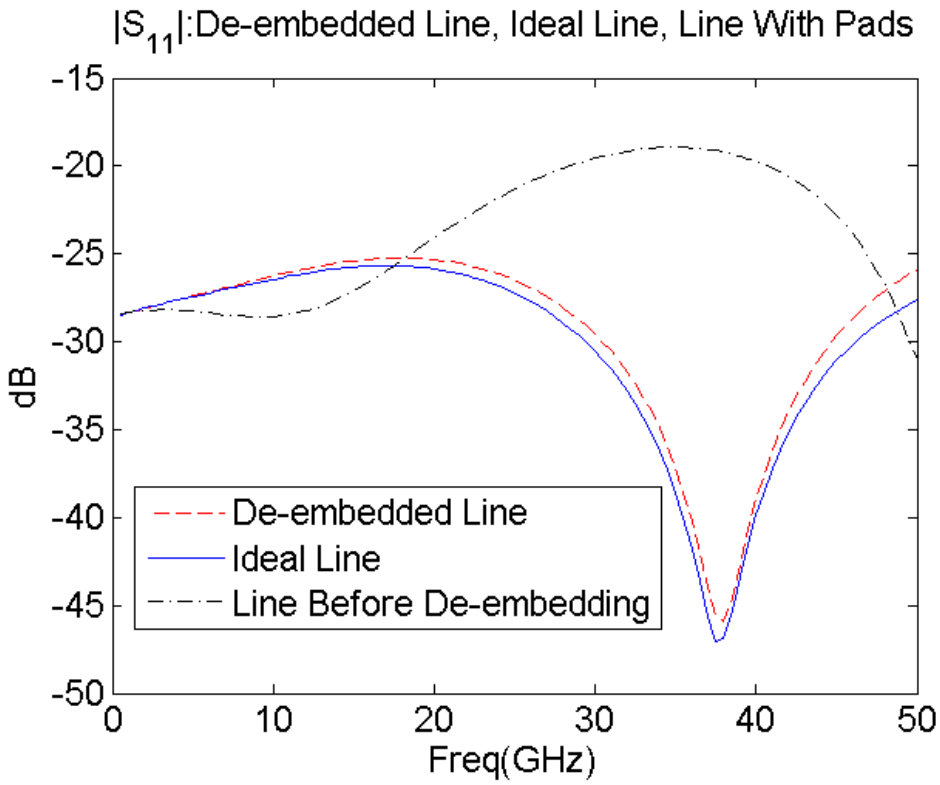

Figure 4.7: Hybrid De-embedding Results for 2L-Li=1900um (S_{11})

4.2 MEASUREMENT VERIFICATION OF LUMPED METHODS

After verifying the lumped methods with simulations, actual measurements were used to further test the robustness of the methods. Measurements were conducted with a Summit 9000 Microprobe Station, a 50 GHz Agilent PNA (Model N5245A), and GSG style, 100um pitch, Infinity Probes from Cascade Microtech. Unfortunately, all the lumped methods failed with measurement data from the IC. An example is given in Figures 4.8 and 4.9 for the L-2L method.

The figures show that the de-embedded data is very unstable and tends to closely follow the original line with pads. Similar trends were shown for both the

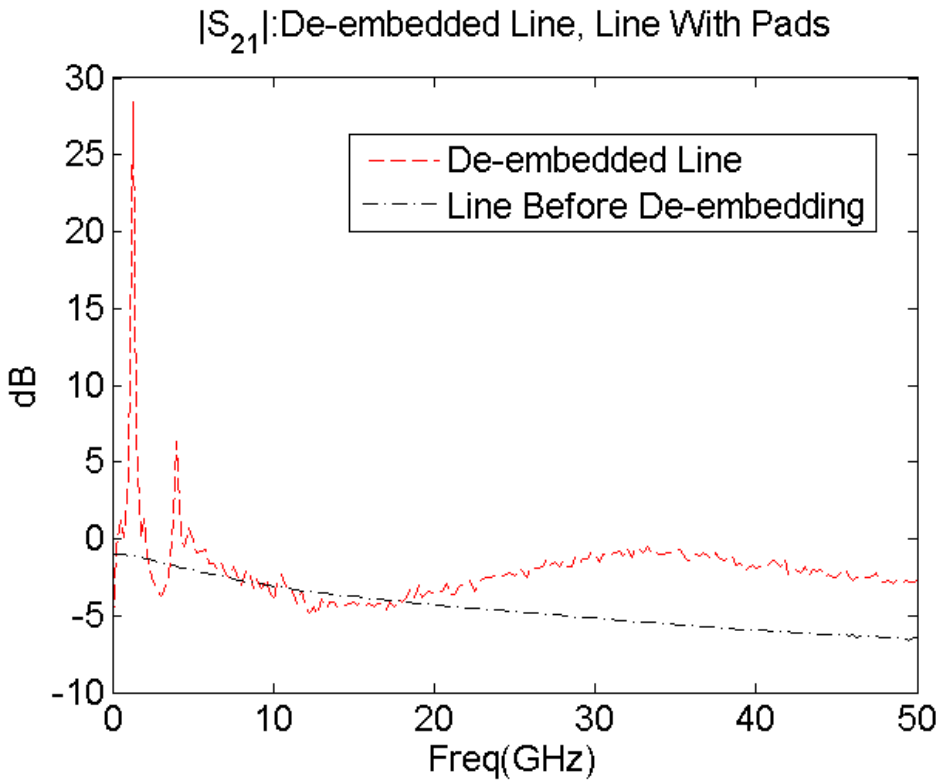

Figure 4.8: L-2L (Meas) De-embedding Results for 2L-L=1000um (S_{21})

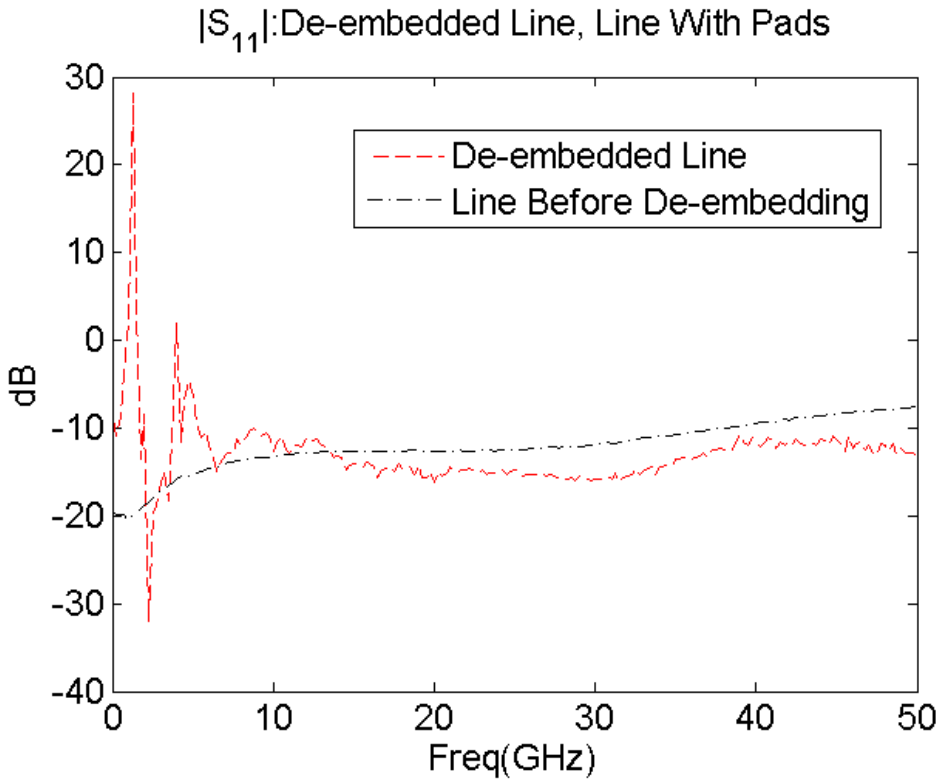

Figure 4.9: L-2L (Meas) De-embedding Results for 2L-L=1000um (S_{11})

LiLj method and the Hybrid method. No comparison can be drawn between the de-embedded line and the ideal line, obviously, because the ideal line cannot be measured, hence the purpose of de-embedding.

4.3 COMMENTS CONCERNING LUMPED METHOD FAILURES

The reason for the lumped models failing in the measurement environment is not altogether clear. One reason could be an improper measurement setup. Much akin to a full-wave simulation port setup, actual measurement setups can be plagued by all sorts of various issues. Some issues experienced in the work for this thesis included:

- How to properly mount the un-packaged IC to a substrate that was big enough to be held by the vacuum system?
- How to ensure that the IC remained planar after being mounted to a bigger substrate?
- How to ensure that the probes properly contacted the IC probing pads?
- How to ensure the probes were operating properly?
- How to identify if there were issues with the VNA ports, precision cables, or adapters that were used in the setup?

However, the measurement setup is not believed to be the culprit in the failure of the lumped element de-embedding methods. The first measurement attempts indicated that one port exhibited a noise fluctuation as compared to the other port. After flipping the IC around during a measurement, and after using two different ports on a four port VNA, the noise issue persisted on the same "measurement" port. These facts strongly suggested a problematic probe. Therefore, a new set of probes were

used to repeat the measurements. The results indicated a similar response as compared to the first set of probes, just without the noise issue. Finding that the results followed the same trends, minus the noise issue, it is believed that the measurement setup was proper since the trends in the results were repeatable. Of course, the setup issues (if any) could have just been repeated as well, though this seems less likely.

Another option for the failure of the lumped element de-embedding methods could be that the methods are too sensitive to the noise that is inherent in an actual measurement environment. For simulations, a rather small number of sample points are solved and then smoothly connected using interpolation. For measurements, many sample points are taken that fluctuate in such a fashion that a smooth interpolation is not possible. Additionally, simulations are considered ideal conditions, with no unintentional environmental effects.

A final option for the lumped element method failures in measurements could have been from a "false positive" given in simulations. The structures simulated (striplines with simple pad discontinuities) may have been too simple compared to the real physical structures used in measurements. If this were the case, then the simple pad model may have fit well (in terms of physics) with the simple models used by the lumped methods. In other words, for the measured transmission line, there may have been no way to fit the pad structure to the simple 2-Impedance model given in Section 2.1. Of course the above discussed issues can only be taken as speculations; the true cause for de-embedding failures remains unclear.

4.4 SIMULATION VERIFICATION OF NON-LUMPED METHODS

4.4.1 Non-Lumped L-2L Results. The same full-wave models used for the lumped cases were re-used for validating the non-lumped methods. The only aspect of the models that varied was the length of the transmission lines.

Figure 4.10 shows the de-embedding results for the Non-Lumped L-2L Method for the special case of knowing that the transmission line embedded between the pads had a characteristic impedance very close to 50 ohms. Here, no information is available for the reflections of the line because the line is assumed to have a characteristic impedance of 50 ohms. The results indicate that the method performs well, up to 50 GHz, in the case of transmission lines having a characteristic impedance close to 50 ohms.

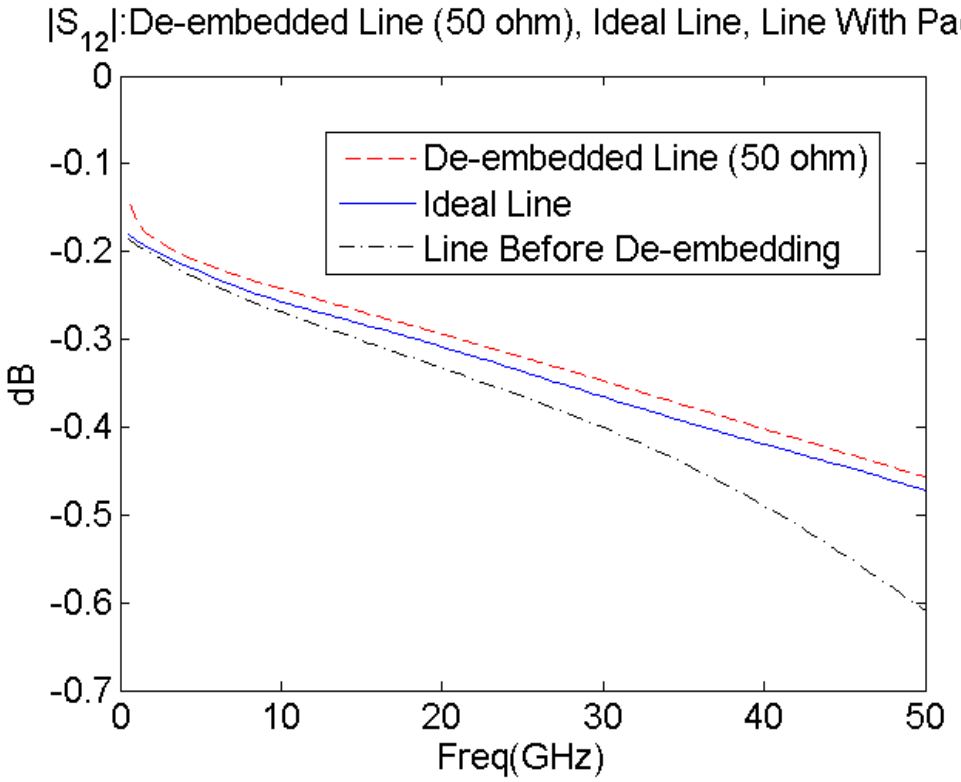

Figure 4.10: Non-Lumped L-2L De-embedding Results for L=1000um (S_{12})

4.4.2 Through Results. Figures 4.11 and 4.12 show the results when the through was used under the assumption that $S_{11} = S_{22}$ for the adapters. The through was generated using the first steps of the L-2L method, as described in Section 2.2.

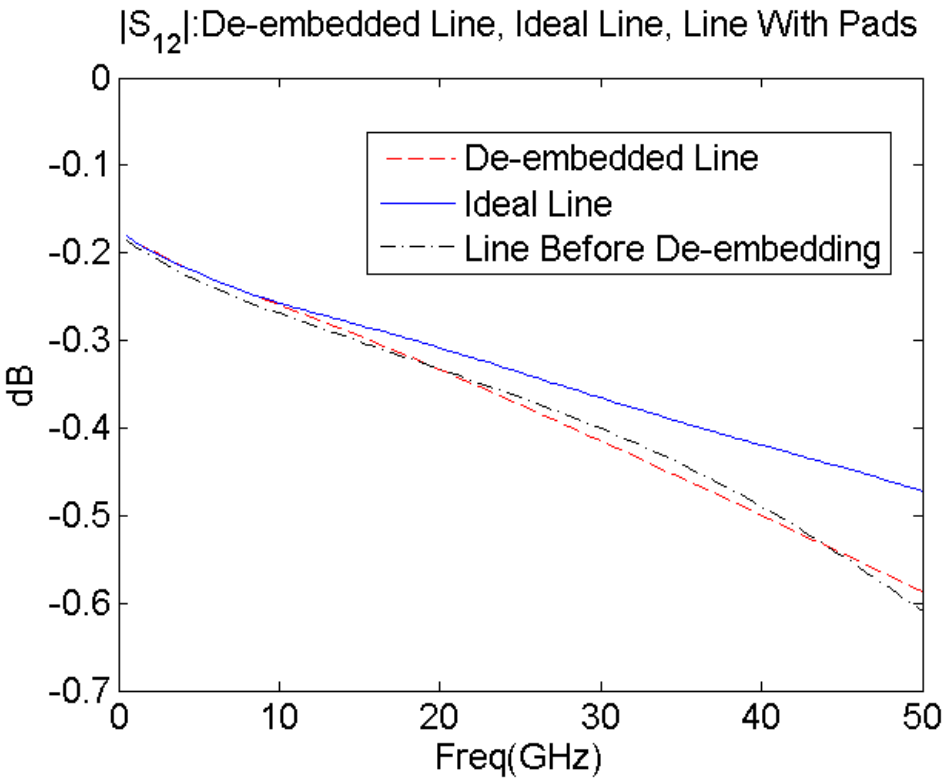

Figure 4.11: Through De-embedding Results for L=1000um (S_{12})

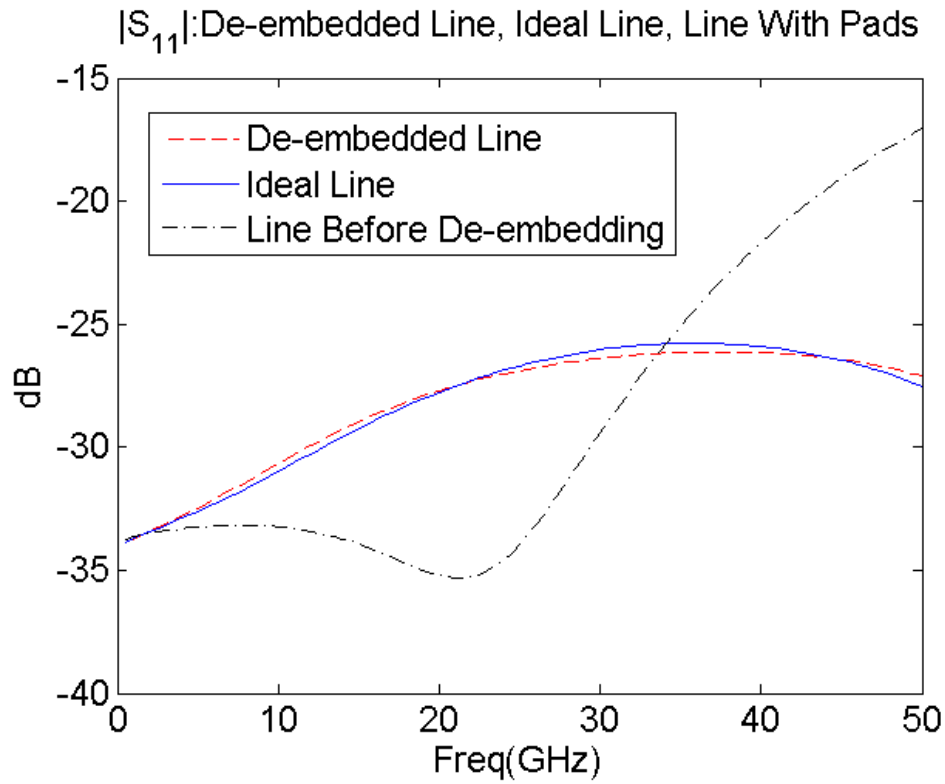

Figure 4.12: Through De-embedding Results for L=1000um (S_{12})

The results of the simulation and algorithm in Figure 4.12 show that the reflections for the de-embedded line match well with the true line up to 50 GHz. In Figure 4.11, S_{12} for the de-embedded line is shown to follow the trend of the line with pads instead of the true line indicating that the assumption that $S_{11} = S_{22}$ can only roughly approximate the characteristics of the pad structures, and thus can only roughly approximate the true characteristics of the transmission line. The through method is a prime example of how ease of use and low mathematical complexity can equate to less accurate de-embedding results.

4.5 MEASUREMENT VERIFICATION OF NON-LUMPED METHODS

4.5.1 Non-Lumped L-2L Method. Measurement results for the non-

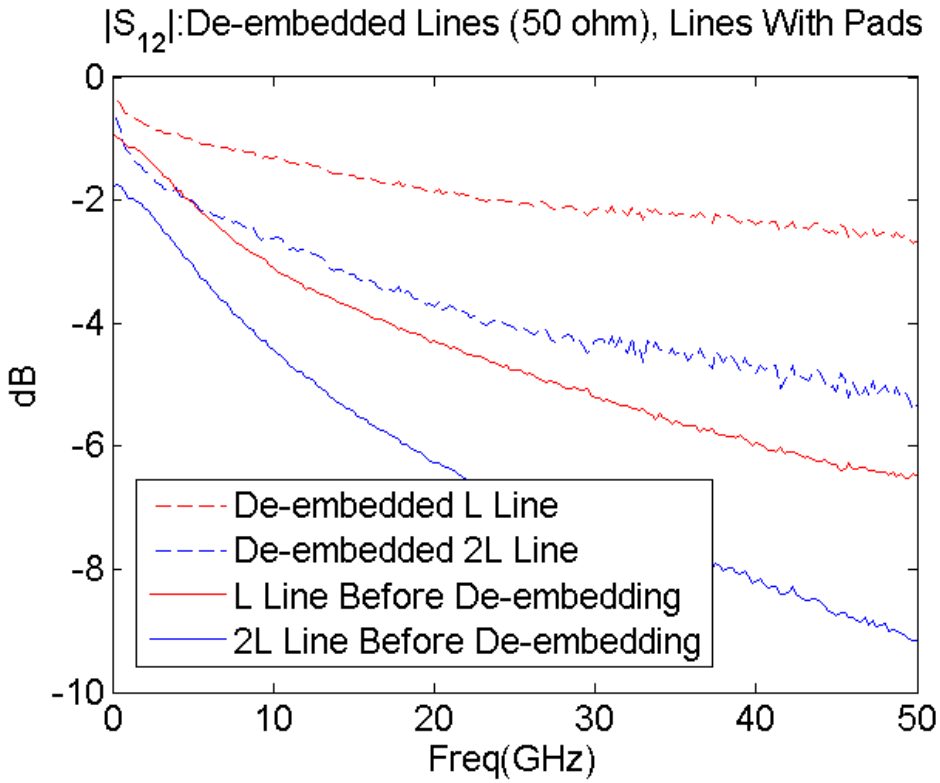

Figure 4.13: Non-Lumped L-2L (Meas) De-embedding Results for L=1000um and 2L=2000um (S_{12})

lumped L-2L method show the expected trends for de-embedding in Figure 4.13. When compared to the measurement results for the through method given in 4.5.2, the method appears to be more accurate. In fact, the trends appear more appropriate for expected transmission line behavior. Comparing the de-embedded L length line and the de-embedded 2L length line, the loss appears proportional to length, and the increase in loss appears proportional to frequency, as is expected for transmission lines.

4.5.2 Through Method. For the through method, de-embedding results were much more stable than the lumped methods and were much more consistent with simulation data than the lumped methods. Again, measurements cannot completely evaluate the preciseness of the de-embedding method since the true lines cannot be measured directly.

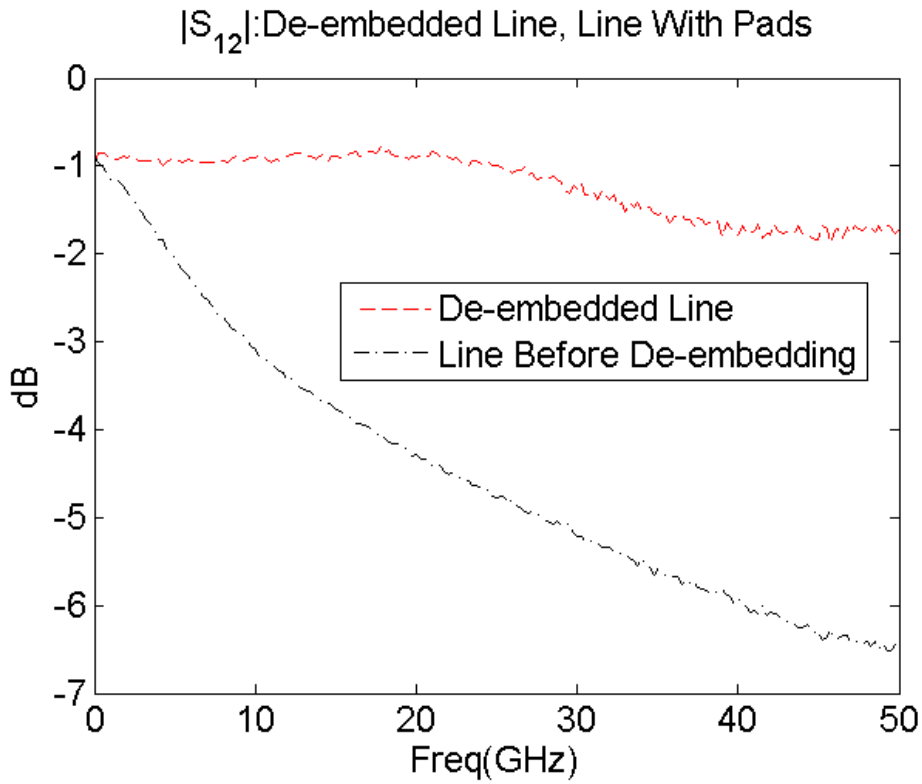

Figure 4.14: Through (Meas) De-embedding Results for L=1000um (S_{12})

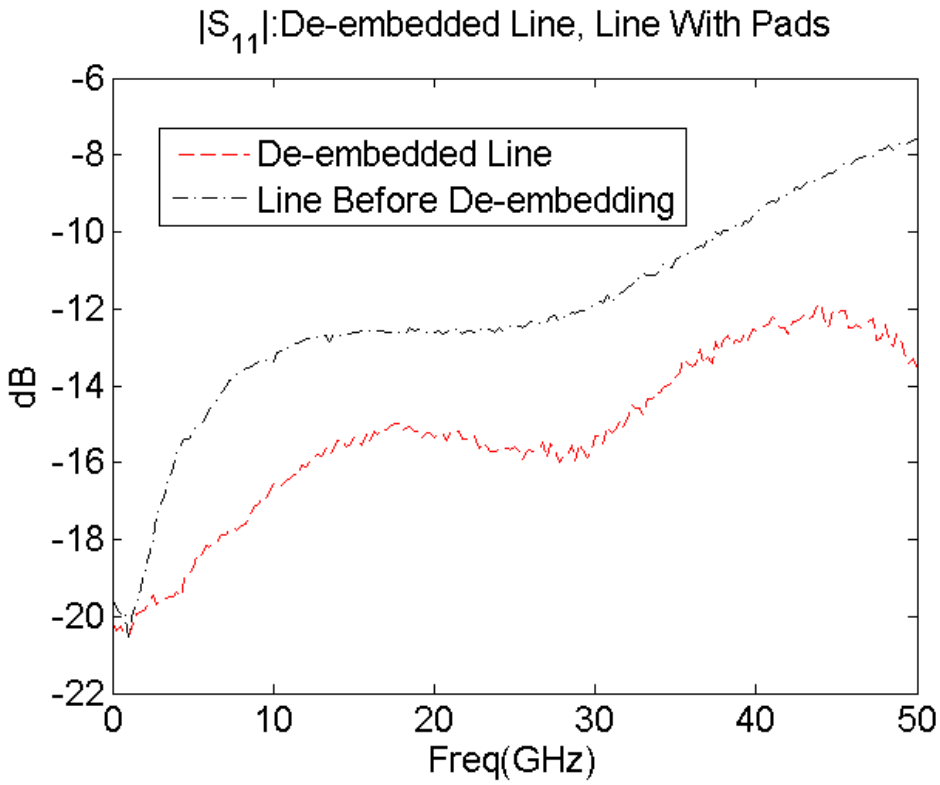

Figure 4.15: Through (Meas) De-embedding Results for L=1000um (S_{11})

Figures 4.14 - 4.16 show that, for the through method (where $S_{11} = S_{22}$ is assumed), measurement results are not as convincing as the non-lumped L-2L method. From an intuition of expected de-embedding behavior, the results of the through method still indicate a high level of reasonableness; post-de-embedding, transmissions and reflections are expected to improve for the de-embedded line as compared to the original line. The results for this method indicate that type of behavior. Compared to the non-lumped L-2L method, though, the transmission behavior of the lines

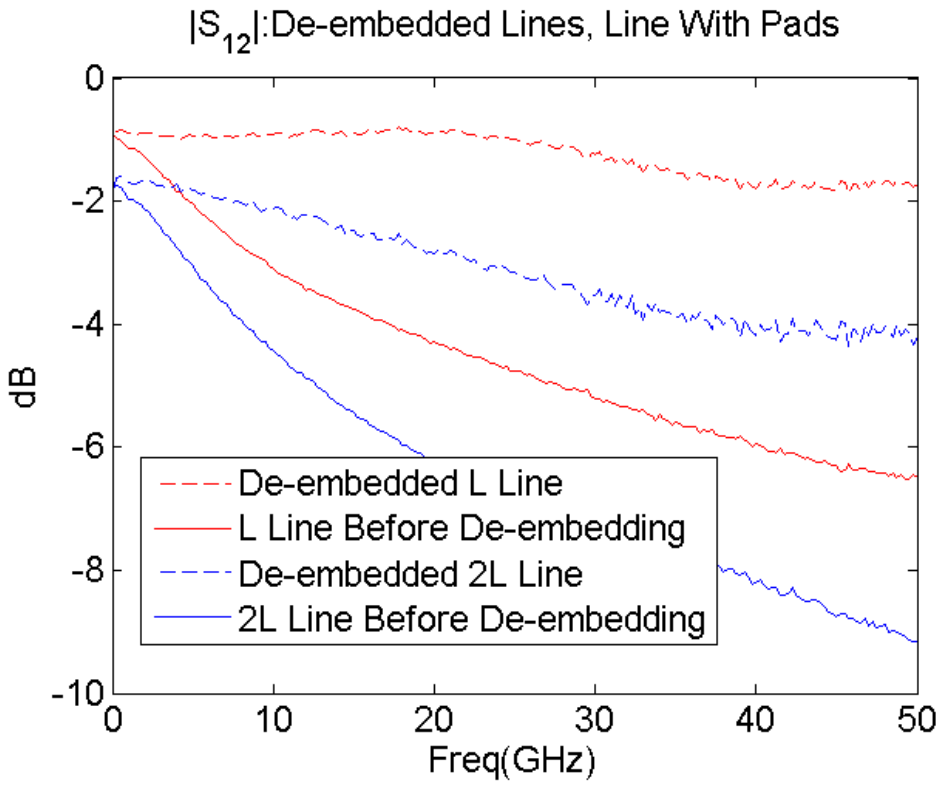

Figure 4.16: Through (Meas) De-embedding Results for L=1000um and 2L=2000um (S_{12})

indicated by the through method is not as indicative of the behavior expected for true transmission lines.

4.6 BEST CHOICE FOR APPLICATION IN DE-EMBEDDING TSVS

After a thorough evaluation of several de-embedding techniques through both simulations and measurements, it is believed that the best choice for de-embedding TSVs is the non-lumped L-2L method. Overall, this method showed the most consistency between simulations and measurements. Additionally, the results of this method were deemed the most reasonable in the case of measurements. The lumped element methods, though they performed extremely well in the simulation environment, did not perform well in the measurement environment. The reason for the

lumped element methods failing remains unclear, but the sole fact that they do not perform well when applied to the same measurement data (in the same way) as the non-lumped methods raises concerns for their use and applicability.

One may argue that the application of the non-lumped method is severely limited without "a priori" knowledge of the characteristic impedance of the embedded transmission lines. However, the TSD and TRL calibration methods use the same 50 ohm delay line assumptions with no hesitation. If care is used during the design phase of silicon transmission lines (and if there is confidence in the fabrication ability of the IC manufacturer), a 50 ohm line approximation may not be a bad assumption. Then the non-lumped L-2L method can be applied without change, but with confidence, for de-embedding purposes.

5. CONCLUSION AND FUTURE WORK

An exhaustive search and evaluation of the most popular de-embedding techniques used with silicon applications was performed in this thesis. In the end, de-embedding is nothing more than an attempt to solve a system of complex equations for a number of complex unknowns. The difficulty in solving these equations arises from the non-linearity and high order nature of these equations. The system of equations is almost always under-determined or over-determined, meaning no unique solution can be found. Instead, no solution or an infinite number of solutions is possible. Using various assumptions, approximations, or constraints, solutions can be chosen that most appropriately approximate reality. This fact is observed throughout all the de-embedding techniques.

For the through method, adapters are assumed to be reciprocal. This assumption still leads to an under-determined system of equations, so adapters are further assumed to only consist of a series impedance and a shunt admittance to allow the solving of the system of equations. The L-2L method uses the same constraints, as it eventually utilizes the through to solve its system of equations. The LiLj method further approximates the pad structures as a single lumped element to facilitate finding a solution to the de-embedding task. As the Hybrid method uses techniques from both the L-2L method and the LiLj method, it too employs the above constraints to solve the de-embedding problem. All the lumped methods were found to fail in actual measurements settings. The belief is that these methods fail because they either make too much of an approximation in solving the system of equations such that the chosen solution drifts far away from the actual solution, or that they are too sensitive to the noisy environment that is inherent to an actual measurement setup.

Overall, the non-lumped techniques are found to be more stable and consistent for de-embedding purposes. Although they impose larger constraints (i.e. requiring lines to be exactly 50 ohms or forcing adapters to be electrically symmetric), the added complexity of modeling adapters as error networks is believed to capture the effects of the adapter more accurately than lumped model approximations. So accuracy comes at the cost of complexity.

In comparison to PCB de-embedding techniques, silicon de-embedding techniques are further complicated by problems arising from ultra small geometries and imperfections in manufacturing processes (i.e. the inability to consistently and accurately create precision measurement standards including opens, shorts, and resistors).

As with any complex problem, many techniques may exist that attempt to solve the problem. This is the case for calibration and de-embedding. The work of this thesis aimed to show that calibration and de-embedding processes are very complex methods that cannot blindly be employed. Assumptions, constraints, environment, and setup must always be thoroughly evaluated to choose the best method for solving problems, as is the case with de-embedding and calibration.

Although the revisited non-lumped L-2L method was found to be the best choice method for application to de-embedding TSVs, it is believed that a better method still exists for more accurate de-embedding algorithms. Extensions to the work presented in this thesis could include an exploration of mathematical properties for systems of non-linear equations, an exploration of numerical methods for solving over-determined and under-determined systems, an exploration of forthcoming de-embedding techniques, an exploration of silicon standards (other than transmission lines) for de-embedding, and further developments and improvements to existing de-embedding techniques.

BIBLIOGRAPHY

[1] J. Song, F. Ling, G. Flynn, W. Blood, and E. Demircan, "A de-embedding technique for interconnects," in *Electrical Performance of Electronic Packaging, 2001*, pp. 129–132, 2001.

[2] N. Erickson, K. Shringarpure, J. Fan, B. Achkir, S. Pan, and C. Hwang, "De-embedding techniques for transmission lines: An exploration, review and proposal," in *Electromagnetic Compatibility (EMC), 2013 IEEE International Symposium on*, 2013.

[3] Q.-H. Bu, N. Li, K. Bunsen, H. Asada, K. Matsushita, K. Okada, and A. Matsuzawa, "Evaluation of a multi-line de-embedding technique for millimeter-wave cmos circuit design," in *Microwave Conference Proceedings (APMC), 2010 Asia-Pacific*, pp. 1901–1904, 2010.

[4] A. Mangan, S. Voinigescu, M.-T. Yang, and M. Tazlauanu, "De-embedding transmission line measurements for accurate modeling of ic designs," *Electron Devices, IEEE Transactions on*, vol. 53, no. 2, pp. 235–241, 2006.

[5] N. R. Franzen and R. A. Speciale, "A new procedure for system calibration and error removal in automated s-parameter measurements," in *Microwave Conference, 1975. 5th European*, pp. 69–73, 1975.

[6] B. Bianco, M. Parodi, S. RIDELLA, and F. Selvaggi, "Launcher and microstrip characterization," *Instrumentation and Measurement, IEEE Transactions on*, vol. IM-25, no. 4, pp. 320–323, 1976.

VITA

Nicholas Garrett Erickson was born in August 1989 in Kansas City, Missouri. He received his B.S. degree in Computer Engineering in May 2012, from the Missouri University of Science and Technology in Rolla, Missouri. In June 2012, he started working towards his M.S. degree in Computer Engineering at the Missouri University of Science and Technology. He completed his M.S. degree in December 2013, at the Missouri University of Science and Technology.